

Article

# Multiplicity Dependencies of Midrapidity Transverse Momentum Distributions of Identified Charged Particles in proton-proton Collisions at $(s)^{1/2} = 7$ TeV at the LHC

Khusniddin K. Olimov <sup>1,\*</sup> , Fu-Hu Liu <sup>2,\*</sup> , Kobil A. Musaev <sup>1</sup> and Maratbek Z. Shodmonov <sup>1</sup>

<sup>1</sup> Physical-Technical Institute of Uzbekistan Academy of Sciences, Chingiz Aytmatov Str. 2b, Tashkent 100084, Uzbekistan; qobilmusayev1986@gmail.com (K.A.M.); maratbekshodmonov@yandex.ru (M.Z.S.)

<sup>2</sup> State Key Laboratory of Quantum Optics and Quantum Optics Devices, Collaborative Innovation Center of Extreme Optics, Institute of Theoretical Physics, Shanxi University, Taiyuan 030006, China

\* Correspondence: khkolimov@gmail.com (K.K.O.); fuhuliu@sxu.edu.cn (F.-H.L.)

**Abstract:** Dependencies of midrapidity  $p_t$  distributions of the charged pions and kaons, protons and antiprotons on charged-particle multiplicity density ( $\langle dN_{ch}/d\eta \rangle$ ) in inelastic proton-proton collisions at  $(s)^{1/2} = 7$  TeV at the LHC, measured by ALICE Collaboration, are investigated. The simultaneous minimum  $\chi^2$  fits with the Tsallis function with thermodynamical consistence and the Hagedorn function with included transverse flow have well-described the  $p_t$  spectra of the particle species in the ten studied groups of charged-particle multiplicity density. The effective temperatures,  $T$ , of the Tsallis function with thermodynamical consistence have shown a steady rise with increasing the charged-particle multiplicity in proton-proton collisions at  $(s)^{1/2} = 7$  TeV, in agreement with the similar result obtained recently in proton-proton collisions at  $(s)^{1/2} = 13$  TeV at the LHC. The respective  $T$  versus  $\langle dN_{ch}/d\eta \rangle$  dependence in proton-proton collisions at  $(s)^{1/2} = 7$  TeV is reproduced quite well by the simple power function with the same value ( $\approx 1/3$ ) of the exponent parameter as that extracted in proton-proton collisions at  $(s)^{1/2} = 13$  TeV. The identical power dependence  $T \sim \epsilon^{1/3}$  between the initial energy density and effective temperature of the system has been observed in proton-proton collisions at  $(s)^{1/2} = 7$  and 13 TeV. We have observed that the transverse radial flow emerges at  $\langle dN_{ch}/d\eta \rangle \approx 6$  and then increases, becoming substantial at larger multiplicity events in proton-proton collisions at  $(s)^{1/2} = 7$  TeV. We have estimated, analyzing  $T_0$  and  $\langle \beta_t \rangle$  versus  $\langle dN_{ch}/d\eta \rangle$  dependencies, that the possible onset of deconfinement phase transition in proton-proton collisions at  $(s)^{1/2} = 7$  TeV occurs at  $\langle dN_{ch}/d\eta \rangle \approx 6.1 \pm 0.3$ , which is close to the corresponding recent estimate ( $\langle dN_{ch}/d\eta \rangle \approx 7.1 \pm 0.2$ ) in proton-proton collisions at  $(s)^{1/2} = 13$  TeV. The corresponding critical energy densities for probable onset of deconfinement phase transition in proton-proton collisions at  $(s)^{1/2} = 7$  and 13 TeV at the LHC have been estimated to be  $0.67 \pm 0.03$  and  $0.76 \pm 0.02$  GeV/fm<sup>3</sup>, respectively.

**Keywords:** transverse momentum ( $p_t$ ) distributions; non-extensive Tsallis distribution function; non-extensivity parameter  $q$ ; Hagedorn function with included transverse flow; transverse flow velocity; effective temperature; kinetic freeze-out temperature; onset of deconfinement phase transition in proton-proton collisions



**Citation:** Olimov, K.K.; Liu, F.-H.; Musaev, K.A.; Shodmonov, M.Z. Multiplicity Dependencies of Midrapidity Transverse Momentum Distributions of Identified Charged Particles in proton-proton Collisions at  $(s)^{1/2} = 7$  TeV at the LHC. *Universe* **2022**, *8*, 174. <https://doi.org/10.3390/universe8030174>

Academic Editors: Maria Vasileiou and Erez Etzion

Received: 21 October 2021

Accepted: 7 March 2022

Published: 10 March 2022

**Publisher's Note:** MDPI stays neutral with regard to jurisdictional claims in published maps and institutional affiliations.



**Copyright:** © 2022 by the authors. Licensee MDPI, Basel, Switzerland. This article is an open access article distributed under the terms and conditions of the Creative Commons Attribution (CC BY) license (<https://creativecommons.org/licenses/by/4.0/>).

## 1. Introduction

The widespread use [1–25] of the Tsallis distribution function in high-energy proton-proton collisions is explained by its very good parameterization of the experimental  $p_t$  spectra of hadrons with just a few parameters: the first one—effective temperature ( $T$ ), the second one—parameter of non-extensivity,  $q$ , which accounts for deviation of  $p_t$  distribution from the Boltzmann–Gibbs exponential distribution, and the third parameter—the fitting constant, assumed to be proportional to the system volume. It is important to note

that the Tsallis function has the advantage of being connected through the entropy to thermodynamics, which is not true with other power law distributions [8]. The  $q$  and  $T$  parameters can also be employed for the identification of the system size scaling as well as initial conditions [25].

There are various modifications of the Tsallis function, which have equally well-described the  $p_t$  distributions of final hadrons in proton-proton collisions up to the largest available  $p_t$  values at the Relativistic Heavy Ion Collider (RHIC) and Large Hadron Collider (LHC) experiments [3–10,15]. The non-extensivity parameter,  $q$ , of the Tsallis function has shown quite noticeable sensitivity to the large  $p_t$  region ( $p_t > 3$  GeV/ $c$ ) of the invariant  $p_t$  distributions of hadrons, suggesting the necessity of analyzing the longer  $p_t$  intervals for extracting the more correct  $q$  values [22–24].

The different transverse flow models have been incorporated into Tsallis statistics to describe the  $p_t$  distributions of hadrons in high-energy heavy-ion and proton-proton collisions at the RHIC and LHC. In most cases, the Blast-Wave model with Boltzmann–Gibbs statistics (the BGBW model) [26–28], the Blast-Wave model with Tsallis statistics (the TBW model) [29,30], the Tsallis distribution with transverse flow effect—improved Tsallis distribution [30–32], and the Hagedorn formula (function) with transverse flow [11,16,21,33] have been used to estimate the kinetic freeze-out temperature and transverse expansion velocity.

Most of the works analyzing high-energy collisions with various versions of the Tsallis function and its modified forms, incorporating other model functions, have used separate fits to  $p_t$  distribution of particular particle species in a studied collision. However, as indicated in [34], it is not feasible to assign the physical meaning to collective properties, such as kinetic freeze-out temperature or radial transverse flow velocity, extracted from separate model fits to each particle type. The simultaneous model fits to  $p_t$  distributions of various particle species in a studied collision system, performed by keeping the temperature and transverse flow velocity as the common (shared) fitted parameters for all particle species, can produce the physically meaningful collective parameters of a collision system [16,21,33,34]. The combined (global) fits have proved to be quite efficient for the extraction of collective properties and the comparison of different collision systems with the help of few parameters [16,21,33,34].

The modern LHC experiments have the goal to create the Quark-Gluon Plasma (QGP) in collisions of heavy ions at high energies to investigate the various properties of QGP matter, which is assumed to have been created a few microseconds after the so-called “Big Bang”, thought to be a starting point for the birth of our Universe. Nonetheless, analysis of tiny  $p + p$  collision systems at high energies is also important and interesting. Such analyses are needed not only because the results from proton-proton collisions are used as a baseline for the investigation of heavy-ion collisions, but also to study the collective properties of a system produced in proton-proton collisions at the largest energies achieved at modern collider experiments [15]. The observations [21,35–50] of different QGP signals in high-multiplicity proton-proton collisions at the LHC, including strong similarity and resemblance of their collective properties to those of heavy ions, serve as a good motivation to further investigate the high-energy proton-proton collisions.

In the present article, we analyze the midrapidity (mid- $y$ )  $p_t$  spectra of given particle species at ten groups of the average charged-particle (pseudo-rapidity) multiplicity density ( $\langle dN_{ch}/d\eta \rangle$ ) in proton-proton collisions at  $(s)^{1/2} = 7$  TeV at the LHC, measured by the ALICE collaboration and included in [45]. The goal of the present paper is to extract information on the evolution of collective parameters of the  $p + p$  system with changing  $\langle dN_{ch}/d\eta \rangle$  through combined (simultaneous) fits of  $p_t$  distributions of the charged pions and kaons, protons and antiprotons in each group of  $\langle dN_{ch}/d\eta \rangle$ , applying the Tsallis distribution with thermodynamical consistence and the Hagedorn function with included transverse flow implemented over the entire measured long  $p_t$  region. The present work follows and uses the same analysis methods as the recent paper [21], in which the mid- $y$   $p_t$  distributions of the same species of particles at ten different groups of  $\langle dN_{ch}/d\eta \rangle$  in proton-proton collisions at  $(s)^{1/2} = 13$  TeV at the LHC, measured by ALICE collaboration

and presented in [51], have been investigated. Therefore, the results obtained in the present work for proton-proton collisions at  $(s)^{1/2} = 7$  TeV are compared systematically with the corresponding results in [21] extracted for proton-proton collisions at  $(s)^{1/2} = 13$  TeV.

## 2. The Data and Methods

ALICE collaboration has selected [45] inelastic proton-proton collision events at  $(s)^{1/2} = 7$  TeV with at least one produced charged particle in the pseudo-rapidity region  $|\eta| < 1$ , which make up around 75% of the total inelastic cross-section. To study the dependence of light-flavor hadron production on multiplicity, the selected collision events have been divided into event classes (groups) according to the total charge accumulated in two V0 detectors (V0M amplitude). The V0M amplitude scales linearly with the total number of the charged particles produced in the pseudo-rapidity window corresponding to acceptance of V0 scintillators [45]. The respective average charged-particle pseudo-rapidity densities,  $\langle dN_{ch}/d\eta \rangle$ , in each class of events have been measured at mid-pseudo-rapidity ( $|\eta| < 0.5$ ). The low  $p_t$  part of the particle spectra has been reconstructed in the rapidity interval  $|y| < 0.5$ , while the high  $p_t$  part has been extracted in the pseudo-rapidity range  $|\eta| < 0.8$  in order to make use of the full statistics of inelastic proton-proton collisions [45]. The average charged-particle multiplicity density and corresponding fractions of inelastic cross-sections for different groups of event multiplicity are shown in Table 1. The  $p_t$  ranges [45] of midrapidity  $p_t$  distributions in inelastic proton-proton collisions at  $(s)^{1/2} = 7$  TeV are as follows: [0.1–20.0] GeV/c for  $\pi^+ + \pi^-$ , [0.2–20.0] GeV/c for  $K^+ + K^-$ , and [0.3–20.0] GeV/c for  $p + \bar{p}$ . These  $p_t$  ranges coincide with those measured [21] by ALICE collaboration at midrapidity in ten groups of  $\langle dN_{ch}/d\eta \rangle$  in inelastic proton-proton collisions at  $(s)^{1/2} = 13$  TeV.

**Table 1.** The mean charged-particle multiplicity density and fraction of inelastic cross-section in ten multiplicity groups in inelastic proton-proton collisions at  $(s)^{1/2} = 7$  TeV.

V0M Mult. Class	$\langle dN_{ch}/d\eta \rangle$	$\sigma/\sigma_{\text{INEL}>0}$ (%)
I	$21.3 \pm 0.6$	0–0.95
II	$16.5 \pm 0.5$	0.95–4.7
III	$13.5 \pm 0.4$	4.7–9.5
IV	$11.5 \pm 0.3$	9.5–14
V	$10.1 \pm 0.3$	14–19
VI	$8.45 \pm 0.25$	19–28
VII	$6.72 \pm 0.21$	28–38
VIII	$5.40 \pm 0.17$	38–48
IX	$3.90 \pm 0.14$	48–68
X	$2.26 \pm 0.12$	68–100

It is well-known that the high  $p_t$  part of the  $p_t$  spectra of particles in high-energy nucleon–nucleon collisions can be reproduced well by the QCD-inspired Hagedorn function [52]:

$$\frac{d^2N}{2\pi N_{ev} p_t dp_t dy} = C \left( 1 + \frac{m_t}{p_0} \right)^{-n} \tag{1}$$

where  $C$  is the normalization constant,  $p_0$  and  $n$  are free parameters,  $m_t = \sqrt{p_t^2 + m_0^2}$  is the transverse energy, and  $m_0$  is the rest mass of a particle. As mentioned above, the various forms of the Tsallis function [1,2] can well-reproduce the  $p_t$  and  $m_t$  spectra of particles in proton-proton collisions at high energies [3–13,22,53]. In its simplest version [10,11,20], the Tsallis function is given at mid- $y$  ( $y \approx 0$ ) by:

$$\frac{d^2N}{2\pi N_{ev} p_t dp_t dy} = C_x \left( 1 + (q-1) \frac{m_t}{T} \right)^{-1/(q-1)} \tag{2}$$

where  $C_x$  is the normalization constant,  $T$  is the effective temperature, and  $q$  is the non-extensivity parameter, characterizing the deviation of  $p_t$  distribution from the exponential Boltzmann–Gibbs distribution. The function in Equation (2) is called a non-extensive generalization of the Boltzmann–Gibbs distribution ( $\sim \exp(-\frac{E}{T})$ ), with the  $q$  parameter added to the temperature parameter. The parameter  $q$  is assumed to also be a measure of non-thermalization [54]. When  $q$  approaches one (1), the Tsallis function tends to the usual Boltzmann–Gibbs distribution. The degree of system thermalization increases as  $q$  approaches one.

Compared to various versions of Tsallis distributions, the following one [3,9,10] at mid- $y$  leads to consistent thermodynamics for the pressure, energy density, and particle number:

$$\frac{d^2N}{2\pi N_{ev} p_t dp_t dy} = C_q m_t \left(1 + (q - 1) \frac{m_t}{T}\right)^{-q/(q-1)} \tag{3}$$

which we call the Tsallis function with thermodynamical consistence in the present analysis. The values of  $T$ , extracted from Tsallis function (Equations (2) and (3)) fits, represent the effective temperatures, which include contributions of both the thermal motion and collective expansion effects. To separate these two factors, the transverse flow velocity is incorporated into the Tsallis distribution function. It has been demonstrated in [10,16] that the Tsallis distribution with thermodynamical consistence, provided in Equation (3), results in noticeably smaller values of  $T$  compared to  $T$  obtained using the simple non-consistent Tsallis function in Equation (2). This is due to the additional  $m_t$  term in Equation (3).

The functions represented by Equations (1) and (2) are mathematically equivalent when making substitutions,  $n = 1/(q - 1)$  and  $p_0 = nT$ . The larger  $n$  values correspond to lower  $q$  values. For the quark-quark point scattering,  $n \approx 4$ , and the parameter  $n$  becomes larger in case of the multiple scattering centers involved [6,55,56]. To embed the effective temperature,  $T$ , the function in Equation (1) is modified, setting  $p_0 = nT$ :

$$\frac{d^2N}{2\pi N_{ev} p_t dp_t dy} = C \left(1 + \frac{m_t}{n T}\right)^{-n} \tag{4}$$

In the present work, we include the transverse flow into Equation (4) by using the transformation  $m_t \rightarrow \langle \gamma_t \rangle (m_t - p_t \langle \beta_t \rangle)$ , as also performed in [11,15,16,21,33]. Then, Equation (4) is modified to:

$$\frac{d^2N}{2\pi N_{ev} p_t dp_t dy} = C \left(1 + \langle \gamma_t \rangle \frac{(m_t - p_t \langle \beta_t \rangle)}{n T_0}\right)^{-n} \tag{5}$$

Here,  $\langle \gamma_t \rangle = 1/\sqrt{1 - \langle \beta_t \rangle^2}$ ,  $\langle \beta_t \rangle$  is the mean transverse flow velocity, and  $T_0$  is an estimated kinetic freeze-out temperature. We call the function in Equation (5) the Hagedorn function with included transverse flow in the present work.

Successful analysis, using the function in Equation (5), of  $p_t$  distributions of particles in collisions at high energies has been performed in [11,15,16,21,33]. The model represented by the function in Equation (5) is a powerful tool, which probes the long  $p_t$  ranges of particles, allowing to compare different collision systems using few parameters [15,16,21,33]. The global parameters  $\langle \beta_t \rangle$  and  $T_0$  obtained in [33] in central Cu + Cu, Au + Au, and Pb + Pb collisions at mid- $y$  at  $(s_{nn})^{1/2} = 200\text{--}2760$  GeV at the RHIC and LHC, applying the modified Hagedorn function in Equation (5) over the long  $p_t$  range, have reproduced all the observed dependencies of  $\langle \beta_t \rangle$  and  $T_0$  on  $\langle N_{part} \rangle$  and  $(s_{nn})^{1/2}$ , extracted using three different transverse expansion (blast-wave) models in the low  $p_t$  range. The values of  $\langle \beta_t \rangle$  in the most central (0–5%) Pb + Pb collisions at  $(s_{nn})^{1/2} = 2.76$  and 5.02 TeV, extracted using the function in Equation (5) over long  $p_t$  ranges in [16], have agreed within fit errors with the respective values of  $\langle \beta_t \rangle$ , obtained by ALICE collaboration in the most central (0–5%) Pb + Pb collisions at  $(s_{nn})^{1/2} = 2.76$  and 5.02 TeV in [34] and [57], respectively, using the combined Boltzmann–Gibbs blast-wave fits applied over low  $p_t$  regions. Simultaneous fits

with the modified Hagedorn function in Equation (5), applied over long  $p_t$  intervals in [16], have confirmed that  $\langle\beta_t\rangle$  grows and  $T_0$  decreases with increasing the collision centrality in Pb + Pb collisions at  $(s_{nn})^{1/2} = 2.76$  and 5.02 TeV, which agrees well with the similar result of ALICE collaboration obtained from combined Boltzmann–Gibbs blast-wave fits in the low  $p_t$  ranges in the same collisions in [34,57].

In the present analysis, for the description of  $p_t$  distributions,  $d^2N/(N_{ev}dp_tdy)$ , of the charged particles in ten groups of event multiplicity in inelastic proton-proton collisions at  $(s)^{1/2} = 7$  TeV, we used the Tsallis function with thermodynamical consistence (Equation (3)) in the following form:

$$\frac{d^2N}{N_{ev}dp_tdy} = 2\pi C_q p_t m_t \left(1 + (q-1) \frac{m_t}{T}\right)^{-\frac{q}{q-1}} \quad (6)$$

Similarly, to describe the  $p_t$  spectra,  $d^2N/(N_{ev}dp_tdy)$ , of particles in the present work, we applied the Hagedorn function with included transverse flow (Equation (5)) in the following form:

$$\frac{d^2N}{N_{ev}dp_tdy} = 2\pi C p_t \left(1 + \langle\gamma_t\rangle \frac{(m_t - p_t \langle\beta_t\rangle)}{nT_0}\right)^{-n} \quad (7)$$

In the present work, the simultaneous fits by the model functions of  $p_t$  distributions of all studied particle types in each group of  $\langle dN_{ch}/d\eta \rangle$  have been conducted using the Nonlinear Curve Fitting of the Origin 9.1 Graphing and Data Analysis Software. The  $T/T_0$  and  $\langle\beta_t\rangle$  are extracted as global (common) parameters for all particle types in the fit procedures.

The combined statistical and systematic errors (added in quadrature) are shown in the figures for the experimental data points. The details for the calculation of systematic errors in the  $p_t$  spectra of the particles are provided in [45]. The minimum  $\chi^2$  fit processes have been conducted accounting for the combined statistical and systematic errors as the weights  $(1/(\text{error})^2)$  for data points. During fits of  $p_t$  distributions of the charged pions, the range  $p_t < 0.5$  GeV/ $c$ , containing significant contribution from decays of baryon resonance, has been excluded, as is also the case in [15,16,21,33,34,57]. It is important to mention that in the present work, we used the same model functions, presented in Equations (6) and (7), and identical fitting  $p_t$  ranges for the studied particle species as used in recent work [21] for proton-proton collisions at  $(s)^{1/2} = 13$  TeV.

### 3. Analysis and Results

The results extracted from simultaneous minimum  $\chi^2$  fits by the Tsallis function with thermodynamical consistence (Equation (6)) of  $p_t$  distributions of the studied particle types in various groups of  $\langle dN_{ch}/d\eta \rangle$  in proton-proton collisions at  $(s)^{1/2} = 7$  TeV are shown in Table 2. The parameter  $T$  is extracted as a shared (common) fitted parameter for all the particle species during the combined fitting procedures by Equation (6) in each group of  $\langle dN_{ch}/d\eta \rangle$ . The results of this global fitting procedure are shown on Figure 1 for four different groups of  $\langle dN_{ch}/d\eta \rangle$ .

**Table 2.** Parameters obtained using combined minimum  $\chi^2$  fits with the Tsallis function with thermodynamical consistence (Equation (6)) of  $p_t$  spectra of particles in various groups of  $\langle dN_{ch}/d\eta \rangle$  in proton-proton collisions at  $(s)^{1/2} = 7$  TeV. The fitted  $p_t$  ranges are [0.5–20.0] GeV/c for  $\pi^+ + \pi^-$ , [0.2–20.0] GeV/c for  $K^+ + K^-$ , and [0.3–20.0] GeV/c for  $p + \bar{p}$ . Here, *n.d.f.* denotes the number of degrees of freedom.

$\langle dN_{ch}/d\eta \rangle$	$q (\pi^+ + \pi^-)$	$q (K^+ + K^-)$	$q (p + \bar{p})$	$T$ (MeV)	$\chi^2/n.d.f.$ ( <i>n.d.f.</i> )
21.3 ± 0.6	1.143 ± 0.001	1.153 ± 0.001	1.133 ± 0.001	131 ± 2	1.85 (114)
16.5 ± 0.5	1.145 ± 0.001	1.154 ± 0.001	1.131 ± 0.001	121 ± 2	1.54 (114)
13.5 ± 0.4	1.146 ± 0.001	1.155 ± 0.001	1.130 ± 0.001	114 ± 1	1.06 (114)
11.5 ± 0.3	1.147 ± 0.001	1.155 ± 0.001	1.128 ± 0.001	109 ± 1	0.79 (114)
10.1 ± 0.3	1.148 ± 0.001	1.155 ± 0.001	1.128 ± 0.001	104 ± 1	0.65 (114)
8.45 ± 0.25	1.149 ± 0.001	1.156 ± 0.001	1.128 ± 0.001	98 ± 1	0.61 (114)
6.72 ± 0.21	1.150 ± 0.001	1.156 ± 0.001	1.125 ± 0.001	91 ± 1	0.45 (114)
5.40 ± 0.17	1.151 ± 0.001	1.157 ± 0.001	1.123 ± 0.001	85 ± 1	0.39 (114)
3.90 ± 0.14	1.151 ± 0.001	1.156 ± 0.001	1.122 ± 0.001	75 ± 1	0.79 (114)
2.26 ± 0.12	1.149 ± 0.001	1.153 ± 0.001	1.114 ± 0.001	57 ± 1	1.00 (114)

Table 3 shows the parameters extracted from combined minimum  $\chi^2$  fits with the Hagedorn function with included transverse flow (Equation (7)) of  $p_t$  distributions of particles in different groups of  $\langle dN_{ch}/d\eta \rangle$  in proton-proton collisions at  $(s)^{1/2} = 7$  TeV. The parameters  $\langle \beta_t \rangle$  and  $T_0$  are extracted as shared (common) fitted parameters for all the particle species during the combined fitting procedures by Equation (7) in each group of  $\langle dN_{ch}/d\eta \rangle$ . Figure 2 illustrates the respective combined minimum  $\chi^2$  fit curves by the Hagedorn function with included transverse flow of mid- $y$   $p_t$  distributions of the studied charged particles in four different groups of  $\langle dN_{ch}/d\eta \rangle$ . Figure 1 and the  $\chi^2/n.d.f.$  values in Table 2 show that the combined fits with the Tsallis function with thermodynamical consistence reproduce quite satisfactory  $p_t$  distributions of hadrons, except that for (anti)protons at high  $p_t$  values in the low-multiplicity events, in ten various groups of  $\langle dN_{ch}/d\eta \rangle$  in proton-proton collisions at  $(s)^{1/2} = 7$  TeV. Similarly, as observed from Figure 2 and the values of  $\chi^2/n.d.f.$  in Table 3, the simultaneous fits with the Hagedorn function with included transverse flow reproduce  $p_t$  distributions of particles quite well, except that for (anti)protons at high  $p_t$  values in the low-multiplicity events, in ten groups of  $\langle dN_{ch}/d\eta \rangle$ .

**Table 3.** Parameters extracted using combined minimum  $\chi^2$  fits with the Hagedorn function with included transverse flow (Equation (7)) of  $p_t$  distributions of particles in various groups of  $\langle dN_{ch}/d\eta \rangle$  in proton-proton collisions at  $(s)^{1/2} = 7$  TeV. The fitted  $p_t$  ranges are [0.5–20.0] GeV/c for  $\pi^+ + \pi^-$ , [0.2–20.0] GeV/c for  $K^+ + K^-$ , and [0.3–20.0] GeV/c for  $p + \bar{p}$ .

$\langle dN_{ch}/d\eta \rangle$	$n (\pi^+ + \pi^-)$	$n (K^+ + K^-)$	$n (p + \bar{p})$	$\langle \beta_t \rangle$ (in $c$ Units)	$T_0$ (MeV)	$\chi^2/n.d.f.$ ( <i>n.d.f.</i> )
21.3 ± 0.6	6.80 ± 0.05	6.61 ± 0.04	8.11 ± 0.06	0.29 ± 0.02	113 ± 3	0.60 (113)
16.5 ± 0.5	6.77 ± 0.05	6.57 ± 0.04	8.13 ± 0.06	0.23 ± 0.02	113 ± 3	0.72 (113)
13.5 ± 0.4	6.78 ± 0.04	6.55 ± 0.04	8.17 ± 0.06	0.18 ± 0.02	114 ± 3	0.63 (113)
11.5 ± 0.3	6.76 ± 0.04	6.52 ± 0.04	8.24 ± 0.06	0.15 ± 0.02	113 ± 3	0.54 (113)
10.1 ± 0.3	6.77 ± 0.04	6.52 ± 0.04	8.24 ± 0.06	0.12 ± 0.02	115 ± 3	0.58 (113)
8.45 ± 0.25	6.74 ± 0.04	6.48 ± 0.04	8.15 ± 0.06	0.07 ± 0.02	115 ± 4	0.74 (113)
6.72 ± 0.21	6.74 ± 0.04	6.47 ± 0.04	8.29 ± 0.06	0.04 ± 0.02	112 ± 3	0.60 (113)
5.40 ± 0.17	6.73 ± 0.04	6.46 ± 0.03	8.40 ± 0.06	0 ± 0.02	108 ± 3	0.56 (113)
3.90 ± 0.14	6.70 ± 0.05	6.49 ± 0.04	8.48 ± 0.09	0 ± 0.03	95 ± 4	0.97 (113)
2.26 ± 0.12	6.75 ± 0.06	6.59 ± 0.05	9.06 ± 0.13	0 ± 0.03	69 ± 4	1.19 (113)

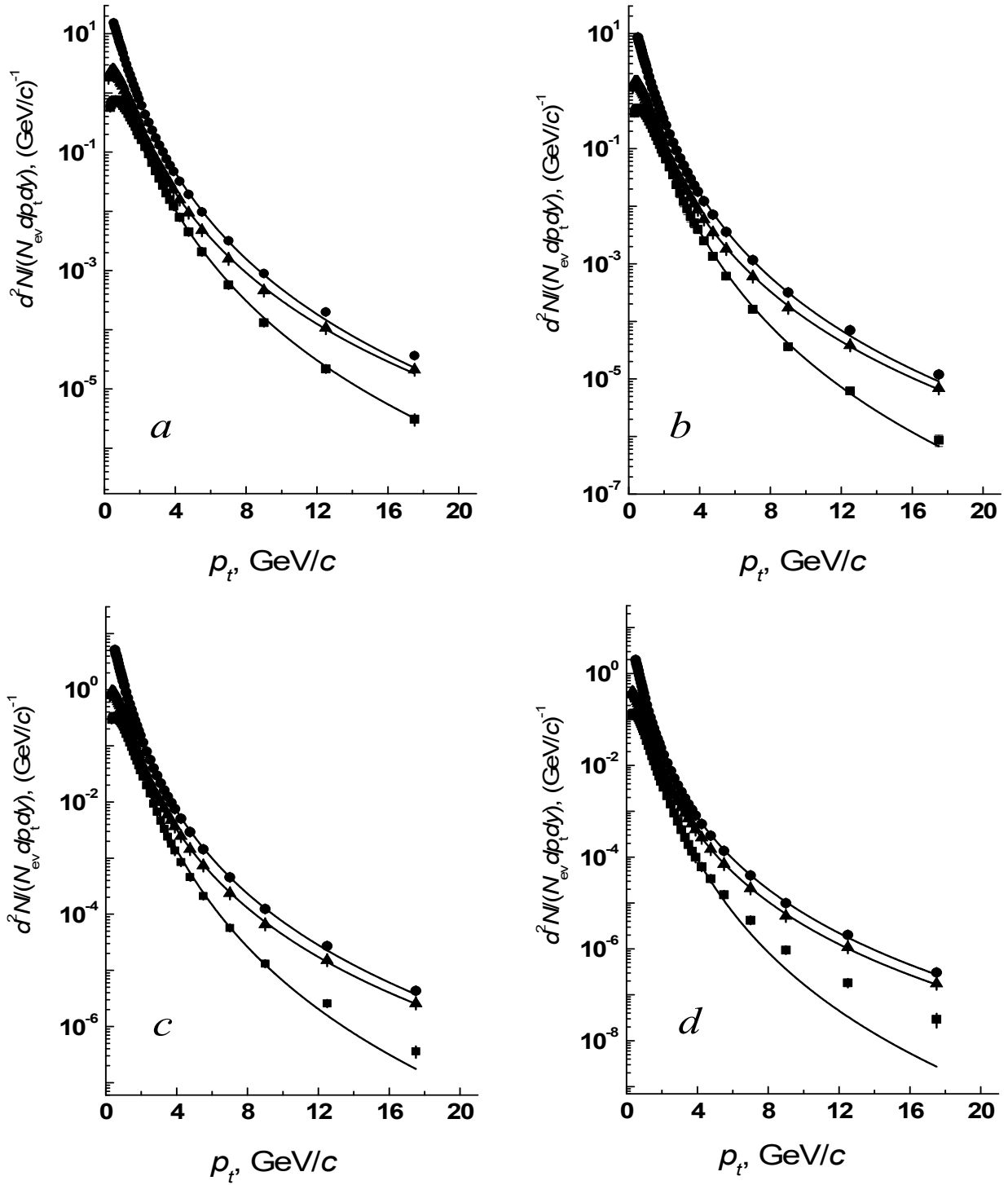


**Figure 1.** The combined minimum  $\chi^2$  fits (solid curves) with the function in Equation (6) of the experimental mid- $y$   $p_t$  distributions of the charged pions ( $\bullet$ ) and kaons ( $\blacktriangle$ ), protons and antiprotons ( $\blacksquare$ ) in proton-proton collisions at  $(s)^{1/2} = 7$  TeV in various groups of  $\langle dN_{ch}/d\eta \rangle$ :  $\langle dN_{ch}/d\eta \rangle = 21.3 \pm 0.6$  (a),  $\langle dN_{ch}/d\eta \rangle = 11.5 \pm 0.3$  (b),  $\langle dN_{ch}/d\eta \rangle = 6.72 \pm 0.21$  (c), and  $\langle dN_{ch}/d\eta \rangle = 2.26 \pm 0.12$  (d). The vertical error bars are combined statistical and systematic errors, dominated by the systematic ones.

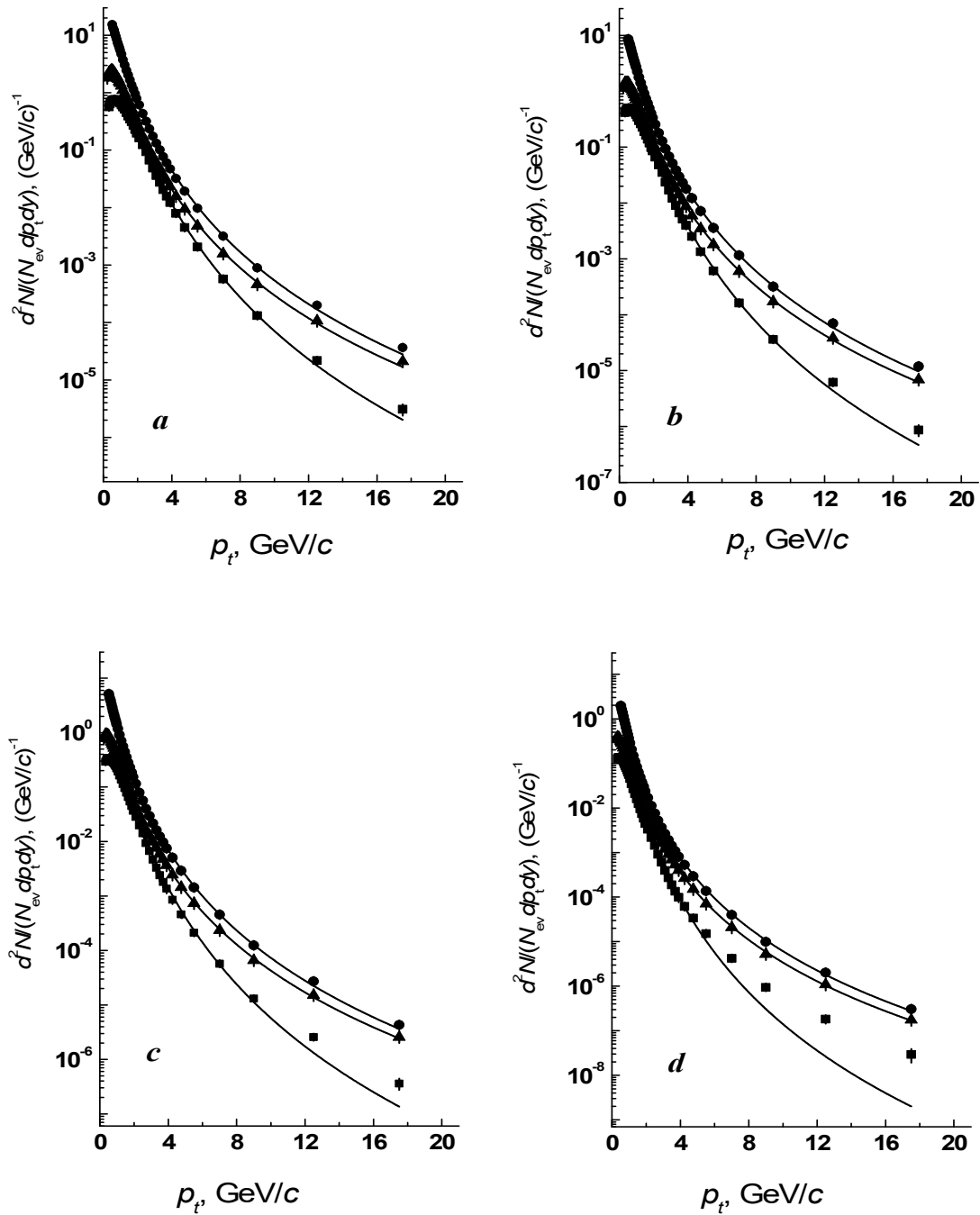


**Figure 2.** The combined minimum  $\chi^2$  fits (solid curves) with the function in Equation (7) of the experimental mid- $y$   $p_t$  distributions of the charged pions ( $\bullet$ ) and kaons ( $\blacktriangle$ ), protons and antiprotons ( $\blacksquare$ ) in proton-proton collisions at  $(s)^{1/2} = 7$  TeV in various groups of  $\langle dN_{ch}/d\eta \rangle$ :  $\langle dN_{ch}/d\eta \rangle = 21.3 \pm 0.6$  (a),  $\langle dN_{ch}/d\eta \rangle = 11.5 \pm 0.3$  (b),  $\langle dN_{ch}/d\eta \rangle = 6.72 \pm 0.21$  (c), and  $\langle dN_{ch}/d\eta \rangle = 2.26 \pm 0.12$  (d). The vertical error bars are combined statistical and systematic errors, dominated by the systematic ones.

As one can see from Figures 1 and 2, the  $p_t$  spectra of (anti)protons could not be described well only in the low-multiplicity  $p + p$  collisions in region  $p_t > 6$ –8 GeV/c. Even in these low-multiplicity (with low  $\langle dN_{ch}/d\eta \rangle < 6$  values)  $p + p$  collision events at  $(s)^{1/2} = 7$  TeV, the quality of the combined fits is quite satisfactory, as one can see from the obtained  $\chi^2/n.d.f.$  values in Tables 2 and 3. We attribute these deviations from model fits in the  $p_t$  spectra of (anti)protons in region  $p_t > 6$ –8 GeV/c in low-multiplicity  $p + p$  collisions to the fact that the protons are already available (as compared to the newly produced pions

and kaons) as initial (colliding) particles, and it requires significantly larger energy to be deposited to the collision system (and hence, a significantly higher degree of thermalization) for the production of new (anti)protons, consisting of three (anti)quarks, as compared to that required for the production of pions and kaons, consisting of two (anti)quarks. Practically no thermalized collective system with collective transverse flow is expected or observed (see Table 3) in peripheral  $p + p$  interactions (with low  $\langle dN_{ch}/d\eta \rangle < 6$  values) with low energy transferred to the system.

Figure 3 illustrates the  $\langle dN_{ch}/d\eta \rangle$  dependencies of the obtained  $q$  and  $T$  parameters of the Tsallis function with thermodynamical consistence for the studied charged particles in proton-proton collisions at  $(s)^{1/2} = 7$  TeV, extracted from simultaneous minimum  $\chi^2$  fits and presented in Table 2. Figure 4 summarizes the  $\langle dN_{ch}/d\eta \rangle$  dependencies of the extracted parameters  $\langle \beta_t \rangle$ ,  $T_0$ , and  $n$  of the Hagedorn function with included transverse flow for the studied particles in proton-proton collisions at  $(s)^{1/2} = 7$  TeV, presented in Table 3. The corresponding data obtained in [21] for the respective particle species in proton-proton collisions at  $(s)^{1/2} = 13$  TeV are also presented in Figures 3 and 4 for comparison. Here, it is worth mentioning the importance of analyzing the behavior of  $\langle \beta_t \rangle$  and  $T_0$  and respective excitation functions [14] because of their relation to map the QCD phase diagram, even though the chemical freeze-out temperature ( $T_{ch}$ ) is normally used in such phase diagrams.

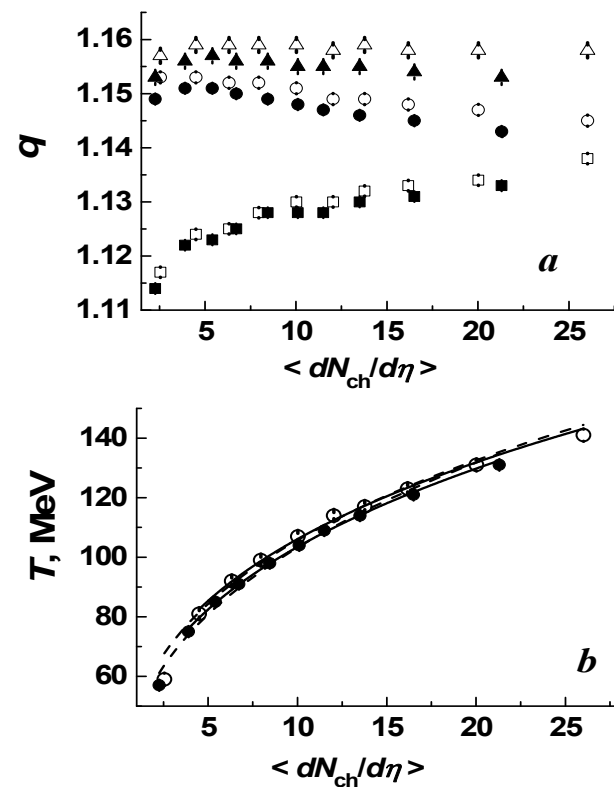


**Figure 3.** (a)—The  $\langle dN_{ch}/d\eta \rangle$  dependencies of the obtained  $q$  values of the Tsallis function with thermodynamical consistence, presented in Table 2, for the charged pions ( $\bullet$ ) and kaons ( $\blacktriangle$ ), protons and antiprotons ( $\blacksquare$ ) in proton-proton collisions at  $(s)^{1/2} = 7$  TeV. (b)—The same for the obtained effective temperatures  $T$  ( $\bullet$ ) of the Tsallis function with thermodynamical consistence, presented in Table 2. The corresponding results extracted from [21] for the respective charged particles in proton-proton collisions at  $(s)^{1/2} = 13$  TeV are shown by the corresponding open (hollow) symbols for comparison. The data points in panel (b) are fitted with the simple power function  $T = A \cdot \langle \frac{dN_{ch}}{d\eta} \rangle^\alpha$ , where  $A$  is the normalization constant, and  $\alpha$  is the exponent parameter. The dashed and solid curves are the simple power function fits of the whole range (10 data points), and of the whole range excluding the first data point (9 data points), respectively.

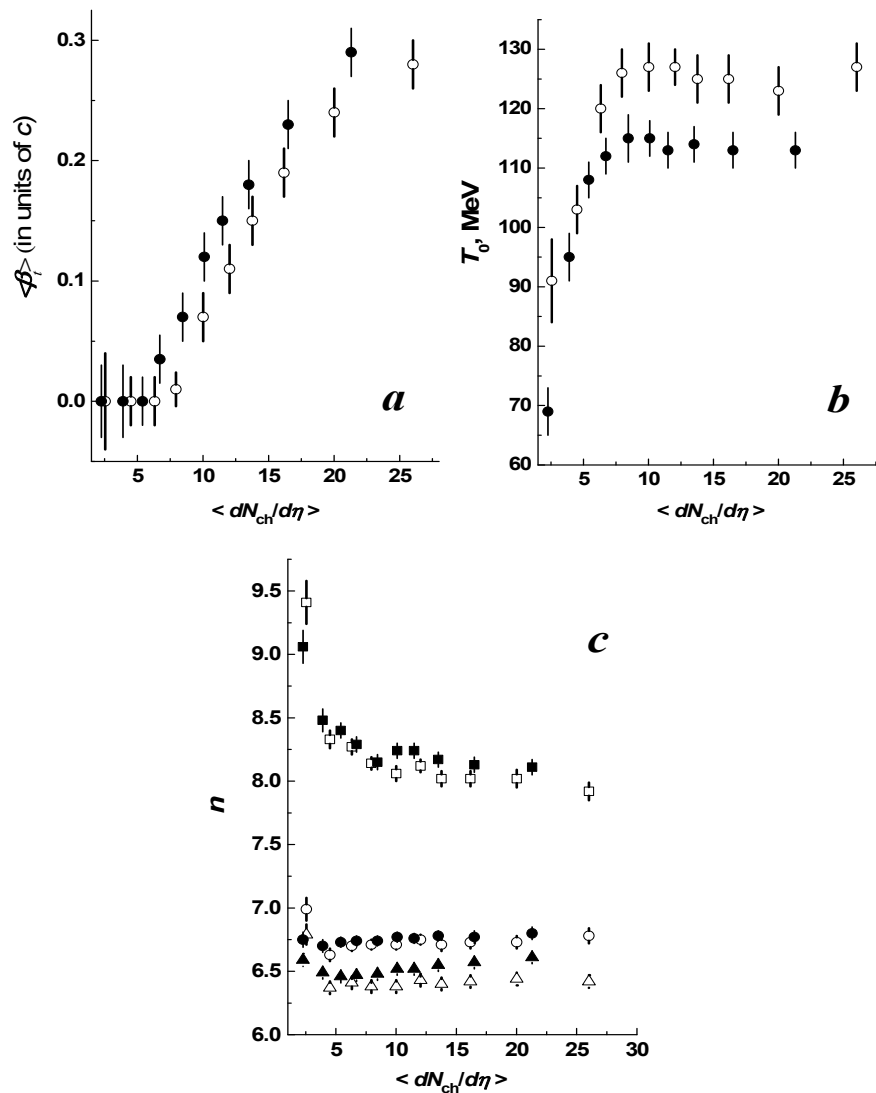


**Figure 4.** The  $\langle dN_{ch}/d\eta \rangle$  dependencies of the obtained  $\langle \beta_t \rangle$  (a) and  $T_0$  (b) parameters (●) of the Hagedorn function with included transverse flow, presented in Table 3, in proton-proton collisions at  $(s)^{1/2} = 7$  TeV. (c)—The same for the obtained  $n$  values of the Hagedorn function with included transverse flow, presented in Table 3, for the charged pions (●) and kaons (▲), protons and antiprotons (■). The corresponding results extracted from [21] for the respective particles in proton-proton collisions at  $(s)^{1/2} = 13$  TeV are shown by the corresponding open (hollow) symbols for comparison.

As observed in Figure 3a, the overall values of  $q$  for mesons (pions and kaons) and baryons (protons and antiprotons) are clearly separated with a  $q(\text{baryons}) < q(\text{mesons})$  relation holding in the entire studied  $\langle dN_{ch}/d\eta \rangle$  region in proton-proton collisions at  $(s)^{1/2} = 7$  and 13 TeV. This is consistent with the  $q(\text{baryons}) < q(\text{mesons})$  relation in minimum bias, high-energy proton-proton collisions obtained earlier in [15,16,22,25]. As observed in Figure 3a, the behavior of  $q$  versus  $\langle dN_{ch}/d\eta \rangle$  dependence for all considered particle types in proton-proton collisions at  $(s)^{1/2} = 7$  TeV is similar to that obtained in proton-proton collisions at  $(s)^{1/2} = 13$  TeV in [21]. However, as observed in Figure 3a, on the whole, the values of  $q$  for the analyzed particle species in proton-proton collisions at  $(s)^{1/2} = 7$  TeV are found to be noticeably lower compared to those in proton-proton collisions at  $(s)^{1/2} = 13$  TeV in the whole analyzed  $\langle dN_{ch}/d\eta \rangle$  range. This can suggest that the systems produced in proton-proton collisions at  $(s)^{1/2} = 7$  TeV are characterized by the noticeably larger degree of equilibrium and thermalization as compared to that in proton-proton interactions at  $(s)^{1/2} = 13$  TeV. This finding is consistent with that of the recent work [16], in which the non-extensivity parameter  $q$  has been shown to increase systematically for all studied particle

species with increasing the energy  $(s)^{1/2}$  of proton-proton collisions from 2.76 to 5.02 TeV. These results suggest that higher-energy proton-proton collisions are characterized by the lower degree of thermalization (larger degree of non-equilibrium).

In [8], the combined  $p_t$  spectra of the charged particles, consisting predominantly of pions, in minimum bias  $p + p$  interactions at wide energy regions  $(s)^{1/2} = 0.54\text{--}7$  TeV have been analyzed using the thermodynamically consistent Tsallis distribution. It has been obtained [8] that  $q$  increases weakly but consistently with beam energy, reaching the highest value  $\approx 1.15$  in minimum bias proton-proton interactions at  $(s)^{1/2} = 7$  TeV. This value agrees with  $q \approx 1.15$  for pions and kaons in Table 2 in the majority of multiplicity classes at  $(s)^{1/2} = 7$  TeV in the present analysis. The effective Tsallis temperature of  $82 \pm 1$  MeV obtained in [8] in minimum bias proton-proton interactions at  $(s)^{1/2} = 7$  TeV agrees within uncertainties with the average effective Tsallis temperature  $\langle T \rangle = 81 \pm 1$  MeV calculated in the present analysis. The average effective Tsallis temperature  $\langle T \rangle$  for minimum bias proton-proton interactions at  $(s)^{1/2} = 7$  TeV in the present work has been calculated using the extracted temperature,  $T_i$ , from Table 2 and the corresponding fraction of events,  $f_i$  (with respect to the total inelastic cross-section), of the  $i$ -th group of  $\langle dN_{ch}/d\eta \rangle$  from Table 1 as follows:  $\langle T \rangle = \sum_{i=1}^{10} (T_i \cdot f_i)$ .

As seen from Figure 3b, the extracted  $T$  values of the Tsallis function with thermodynamical consistence show a similar consistent growth with increasing  $\langle dN_{ch}/d\eta \rangle$  in proton-proton interactions at  $(s)^{1/2} = 7$  TeV as that observed in collisions of protons at  $(s)^{1/2} = 13$  TeV. This result can be explained by the fact that the larger multiplicity collisions are consistent with harder proton-proton collisions, in which a larger amount of energy-momentum is deposited to a system [21]. We have fitted the data points in Figure 3b, extracted from proton-proton collisions at  $(s)^{1/2} = 7$  TeV, employing the simple power function  $T = A \cdot \langle \frac{dN_{ch}}{d\eta} \rangle^\alpha$ , where  $A$  is the normalization constant and  $\alpha$  is the exponent parameter, as was carried out in [21]. Similar to [21], we have conducted the minimum  $\chi^2$  fits by this simple power function in the entire studied  $\langle dN_{ch}/d\eta \rangle$  region, and in the entire  $\langle dN_{ch}/d\eta \rangle$  region excluding the first data point, i.e., excluding the softest (ultra-peripheral) proton-proton collisions. The respective results from minimum  $\chi^2$  fits are presented in Table 4. The corresponding data extracted from [21] for proton-proton interactions at  $(s)^{1/2} = 13$  TeV are also shown in Table 4 for comparison. Figure 3b and  $\chi^2/n.d.f.$  values in Table 4 show that this power function is not able to well-reproduce the  $T$  versus  $\langle dN_{ch}/d\eta \rangle$  dependence in the entire studied region. However, as seen from Figure 3b and values of  $\chi^2/n.d.f.$  from Table 4, the  $T$  versus  $\langle dN_{ch}/d\eta \rangle$  dependence in proton-proton collisions at  $(s)^{1/2} = 7$  TeV is described quite satisfactorily, with the function  $T = A \cdot \langle \frac{dN_{ch}}{d\eta} \rangle^\alpha$  having exponent parameter  $\approx 1/3$  in region  $\langle dN_{ch}/d\eta \rangle > 3$ , when the first data point is excluded from the fit range. This agrees very well, as observed from Figure 3b and Table 4, with the similar result in [21], in which the  $T$  versus  $\langle dN_{ch}/d\eta \rangle$  dependence in proton-proton interactions at  $(s)^{1/2} = 13$  TeV has been described quite well with the function  $T = A \cdot \langle \frac{dN_{ch}}{d\eta} \rangle^\alpha$  with exponent parameter  $\approx 1/3$  in the whole  $\langle dN_{ch}/d\eta \rangle$  region, excluding the first data point.

It was observed from Figure 4a that  $\langle \beta_t \rangle$  values, obtained employing the Hagedorn function with included transverse flow, are essentially zero in the range  $\langle dN_{ch}/d\eta \rangle < 6$  (the first three data points) in proton-proton interactions at  $(s)^{1/2} = 7$  TeV. As observed in Figure 4a, beginning from  $\langle dN_{ch}/d\eta \rangle \approx 6$ , the transverse flow starts emerging and developing, with parameter  $\langle \beta_t \rangle$  growing steadily in region  $\langle dN_{ch}/d\eta \rangle > 6$  until the largest  $\langle dN_{ch}/d\eta \rangle$  values. The corresponding parameter  $T_0$  grows systematically in the low-multiplicity region  $\langle dN_{ch}/d\eta \rangle < 6$  (the first three data points) and does not change within the fit uncertainties in the broad region  $\langle dN_{ch}/d\eta \rangle > 6$  in proton-proton interactions at  $(s)^{1/2} = 7$  TeV. The broad plateau range of  $T_0$  starting at  $\langle dN_{ch}/d\eta \rangle \approx 6$  in Figure 4b goes along with a simultaneous and systematic rise of  $\langle \beta_t \rangle$  with increasing  $\langle dN_{ch}/d\eta \rangle$  in the wide region  $\langle dN_{ch}/d\eta \rangle > 6$  in Figure 4a. The observation that the temperature,  $T_0$ , first rises in the range  $\langle dN_{ch}/d\eta \rangle < 6$ , reaching a wide plateau beginning at  $\langle dN_{ch}/d\eta \rangle \approx 6$ , which matches the

absence of transverse flow at  $\langle dN_{ch}/d\eta \rangle < 6$  and the emergence and systematic increase of  $\langle \beta_t \rangle$  at the wide range  $\langle dN_{ch}/d\eta \rangle > 6$ , suggests the probable onset of deconfinement phase transition at  $\langle dN_{ch}/d\eta \rangle \approx 6$  in proton-proton interactions at  $(s)^{1/2} = 7$  TeV. The  $\langle \beta_t \rangle$  and  $T_0$  versus  $\langle dN_{ch}/d\eta \rangle$  dependencies in collisions of protons at  $(s)^{1/2} = 7$  TeV, as observed from Figure 4a,b, qualitatively match those in collisions of protons at  $(s)^{1/2} = 13$  TeV obtained in [21], with some differences observed in the absolute values of parameters. It is seen in Figure 4a,b that the absolute values of  $\langle \beta_t \rangle$  are noticeably smaller and the  $\langle dN_{ch}/d\eta \rangle$  value for the probable onset of phase transition and the value of  $T_0$  in the plateau region are larger in  $p + p$  collisions at  $(s)^{1/2} = 13$  TeV as compared to those at  $(s)^{1/2} = 7$  TeV. It has been estimated in [21] from the analysis of  $T_0$  and  $\langle \beta_t \rangle$  versus  $\langle dN_{ch}/d\eta \rangle$  dependencies that the expected onset of deconfinement phase transition in proton-proton collisions at  $(s)^{1/2} = 13$  TeV takes place at  $\langle dN_{ch}/d\eta \rangle \approx 7.1 \pm 0.2$ . We have followed a similar procedure as that in [21] to better estimate the critical value of  $\langle dN_{ch}/d\eta \rangle$  for the probable onset of deconfinement phase transition in collisions of protons at  $(s)^{1/2} = 7$  TeV: The critical  $\langle dN_{ch}/d\eta \rangle$  is estimated to be the middle value on the  $\langle dN_{ch}/d\eta \rangle$  axis between the third and fourth points in Figure 4b, which correspond to  $\langle dN_{ch}/d\eta \rangle = 5.40 \pm 0.17$  and  $\langle dN_{ch}/d\eta \rangle = 6.72 \pm 0.21$ , respectively, in Table 1. The respective estimate for the probable onset of deconfinement phase transition in  $p + p$  collisions at  $(s)^{1/2} = 7$  TeV proved to be  $\langle dN_{ch}/d\eta \rangle \approx 6.1 \pm 0.3$ , which is smaller than, but close to, the corresponding  $\langle dN_{ch}/d\eta \rangle \approx 7.1 \pm 0.2$  obtained in  $p + p$  collisions at  $(s)^{1/2} = 13$  TeV in [21].

**Table 4.** Parameters extracted from minimum  $\chi^2$  fits using the simple power function  $T = A \cdot \langle \frac{dN_{ch}}{d\eta} \rangle^\alpha$  of the  $T$  versus  $\langle dN_{ch}/d\eta \rangle$  dependencies in Figure 3b in the whole  $\langle dN_{ch}/d\eta \rangle$  region (I), and in the whole region excluding the first data point (II) with  $\langle dN_{ch}/d\eta \rangle = 2.26 \pm 0.12$  and  $\langle dN_{ch}/d\eta \rangle = 2.55 \pm 0.04$  in proton-proton collisions at  $(s)^{1/2} = 7$  and 13 TeV, respectively. The corresponding data extracted from [21] for proton-proton collisions at  $(s)^{1/2} = 13$  TeV are shown for comparison.

$\langle dN_{ch}/d\eta \rangle$ Fit Range	Collision Type, (s) <sup>1/2</sup>	A (MeV)	$\alpha$	$\chi^2/n.d.f.$ (n.d.f.)
I	$p + p$ , 7 TeV	$45.8 \pm 1.4$	$0.353 \pm 0.013$	3.67 (8)
	$p + p$ , 13 TeV [21]	$49.9 \pm 1.7$	$0.33 \pm 0.01$	3.66 (8)
II	$p + p$ , 7 TeV	$48.7 \pm 0.6$	$0.327 \pm 0.005$	0.37 (7)
	$p + p$ , 13 TeV [21]	$51.5 \pm 0.9$	$0.31 \pm 0.01$	1.05 (7)

As observed in Figure 4c, the  $n$  versus  $\langle dN_{ch}/d\eta \rangle$  dependencies, obtained by employing the Hagedorn function with included transverse flow, in proton-proton collisions at  $(s)^{1/2} = 7$  and 13 TeV [21] approximately match the respective inverse dependencies of the  $q$  parameter for the studied particles in Figure 3a.

#### 4. Further Analysis and Discussion

It has been observed that  $\langle \beta_t \rangle$  becomes considerable at larger multiplicities in proton-proton collisions at  $(s)^{1/2} = 7$  TeV, attaining the maximal value (see Table 3) of  $\langle \beta_t \rangle = 0.29 \pm 0.02$  at the highest studied value of  $\langle dN_{ch}/d\eta \rangle = 21.3 \pm 0.6$ . The transverse flow has been absent in proton-proton collisions in the low-multiplicity region  $\langle dN_{ch}/d\eta \rangle < 6$  (see Table 3 and Figure 4a). These results are consistent with the similar emergence and development of transverse radial flow in higher  $\langle dN_{ch}/d\eta \rangle$  events in collisions of protons at  $(s)^{1/2} = 13$  TeV at the LHC recently deduced in [21]. As shown in Table 1, the  $\langle \beta_t \rangle \approx 0$  events with  $\langle dN_{ch}/d\eta \rangle < 6$  make up around 62% of the total statistics of inelastic proton-proton collisions at  $(s)^{1/2} = 7$  TeV. In recent papers [15,16], almost zero transverse flow velocity has been extracted in minimum bias inelastic proton-proton collisions at  $(s)^{1/2} = 2.76, 5.02,$  and 7 TeV, analyzing mid- $y$   $p_t$  distributions of particles with the Hagedorn function with embedded transverse flow. The practically zero  $\langle \beta_t \rangle$  values obtained in [15,16] in minimum bias inelastic proton-proton interactions at  $(s)^{1/2} = 2.76, 5.02,$  and 7 TeV are likely due to

the dominant fraction of events with low-multiplicity with the absence of transverse flow in the total ensemble of inelastic proton-proton collisions.

The various features of QGP: the enhancement of strangeness [38], hardening of  $p_t$  distributions [39,40], and other QGP characteristics [35–37,41–50,58], obtained in proton-proton collisions at the LHC have been published. The onset of collective radial expansion in proton-proton collisions at  $(s)^{1/2} = 900$  and 7000 GeV at the LHC have been reported in [35]. The emergence and development of transverse radial flow in larger multiplicity proton-proton events at  $(s)^{1/2} = 13$  TeV at the LHC have been reported in [21]. The signatures of an equilibrated and collective system in large-multiplicity proton-proton events at  $(s)^{1/2} = 7$  TeV at the LHC were discovered in [45]. In [38], the integrated yields of strange and multi-strange particles, relative to pions, have been shown to increase significantly with increasing  $\langle dN_{ch}/d\eta \rangle$  in proton-proton interactions at  $(s)^{1/2} = 7$  TeV at the LHC. This has been the first reported finding [38] of strangeness enhancement in large-multiplicity  $p + p$  events. These measurements [38] of ALICE collaboration have proven to be in remarkable agreement with those of  $p + \text{Pb}$  collisions at  $(s_{nn})^{1/2} = 5.02$  TeV at LHC, implying that the observed phenomenon is due to the final system produced in a collision. In large-multiplicity  $p + p$  collisions [38], the strangeness production has reached values similar to those obtained in  $\text{Pb} + \text{Pb}$  collisions at  $(s_{nn})^{1/2} = 2.76$  TeV, in which QGP is created. In a recent analysis [44],  $p_t$  distributions of hadrons as a function of charged-particle multiplicity and transverse sphericity have been investigated, using non-extensive Tsallis statistics and the Boltzmann–Gibbs blast-wave (BGBW) model in collisions of protons at  $(s)^{1/2} = 13$  TeV, with the help of the PYTHIA8 event generator. It has been deduced that the isotropic proton-proton collisions approach to thermal equilibrium, while the jetty events remain far from equilibrium [44].

The recent analyses in [46–50] present convincing explanations regarding the source of thermalization in proton-proton collisions at high energies. Thermal abundances of particle yield in proton-proton collisions at high energies with an exponential component in  $p_t$  distributions of hadrons are considered to be a clear signature of thermalization [46,50,58,59]. Since a few secondary interactions in high-energy proton-proton collisions do not support thermalization via interactions at the final state, the discovery of a thermal feature in proton-proton collisions has been quite surprising [46,50]. The thermalization in high-energy proton-proton interactions has been explained in [46–49] as the process occurring during the rapid quench caused by collisions due to the large extent of quantum entanglement inside the wave functions of partons of colliding protons. Therefore, the effective  $T$  extracted from the  $p_t$  spectra of hadrons depends on momentum transfer, constituting an ultraviolet cutoff of quantum modes resolved by collision [46,50]. In [50],  $p_t$  distributions at various multiplicities of  $\text{Pb} + \text{Pb}$  collisions at  $(s_{nn})^{1/2} = 2.76$  TeV and proton-proton collisions at  $(s)^{1/2} = 7$  TeV have been fitted well by the sum of an exponential and power-like function, represented by thermal-like temperature,  $T_{th}$ , and hard temperature,  $T_h$ . The thermalization caused by quantum entanglement has been confirmed in [50], analyzing the multiplicity dependence of proton-proton and  $\text{Pb} + \text{Pb}$  collision data at the LHC. No thermal radiation is expected in diffractive proton-proton events with a large rapidity gap, because in such events the whole proton wave function becomes involved and entanglement entropy does not occur [50]. It has been indeed found in [46] that the thermal component vanishes in diffractive proton-proton interactions at  $(s)^{1/2} = 13$  TeV, in spite of many hadrons still being created. In the studied proton-proton and  $\text{Pb} + \text{Pb}$  collision data at LHC, the effective thermalization temperature,  $T_{th}$ , proved to be proportional [50] to the hard temperature,  $T_h$ , determined by the average  $p_t$ . The obtained coefficient of proportionality has been shown as being universal and independent from the type of collision [50]. The proportionality between  $T_{th}$  and  $T_h$  has been interpreted as that arising from color source clustering [50]. The  $T_{th}$  and  $T_h$  have been shown to rise with increasing multiplicity of both  $p + p$  and  $\text{Pb} + \text{Pb}$  collisions [50].

The systematic rise of parameter  $T$  (extracted employing the Tsallis function with thermodynamical consistence) with increasing particle multiplicity in proton-proton collisions

at  $(s)^{1/2} = 7$  and 13 TeV [21], as seen from Figure 3b, is in agreement with the increase of  $T_{th}$  with multiplicity in collisions of protons at the LHC in [50]. We have confirmed an interesting result of [21], namely that  $T$  versus  $\langle dN_{ch}/d\eta \rangle$  dependence in collisions of protons at  $(s)^{1/2} = 13$  TeV is described well with the function  $T = A \cdot \langle \frac{dN_{ch}}{d\eta} \rangle^\alpha$  with exponent parameter  $\approx 1/3$ . In the present paper, we have obtained that  $T$  versus  $\langle dN_{ch}/d\eta \rangle$  dependence in  $p + p$  collisions at  $(s)^{1/2} = 7$  TeV is also described quite satisfactorily, with this power function having the exponent parameter  $\approx 1/3$  in the wide region  $\langle dN_{ch}/d\eta \rangle > 3$ . Hence, assuming the proportionality of the charged-particle multiplicity density to the initial energy density ( $\epsilon$ ), it is deduced that  $T \sim \epsilon^{1/3}$  in proton-proton collisions at  $(s)^{1/2} = 7$  and 13 TeV. The linear proportionality of the charged-particle multiplicity density to the initial energy density ( $\epsilon$ ) has been demonstrated in Figure 3 of [42], in which advanced calculations of the initial energy density of  $(s)^{1/2} = 7$  and 8 TeV  $p + p$  collisions have been performed, using the accelerating, exact, and explicit solutions of relativistic hydrodynamics [42]. It is interesting to mention that in a simple model of an ideal gas of massless pions [60], the energy density as a function of temperature is described by the Stefan–Boltzmann form  $\epsilon_\pi = \left(\frac{\pi^2}{10}\right)T^4$ , and hence  $T \sim \epsilon_\pi^{1/4}$ . Comparing  $T \sim \epsilon^{1/3}$  extracted in the present analysis and in [21] with the relation  $T \sim \epsilon_\pi^{1/4}$  for the model of an ideal gas of massless pions, one can see that the energy density dependencies of the effective temperatures of the systems, formed in proton-proton collisions at  $(s)^{1/2} = 7$  and 13 TeV [21], and of the temperature of an ideal gas of massless pions, are compatible with each other due to the closeness of the respective exponent parameters.

Employing the explicit and exact relativistic hydrodynamic solutions, the advanced calculations of initial energy density in minimum bias proton-proton interactions at mid- $y$  at  $(s)^{1/2} = 7$  and 8 TeV at the LHC were performed in [42]. The improved advanced hydrodynamic evaluations [42] of initial energy density in minimum bias proton-proton collisions at mid- $y$  at the LHC have yielded  $\epsilon(7 \text{ TeV}) = 0.645 \text{ GeV}/\text{fm}^3$  and  $\epsilon(8 \text{ TeV}) = 0.641 \text{ GeV}/\text{fm}^3$ , respectively, which are below the critical energy density ( $1 \text{ GeV}/\text{fm}^3$ ) from lattice QCD calculations. These results were extracted using the mean values of the charged-particle multiplicity density at mid- $y$  in minimum bias proton-proton collisions at  $(s)^{1/2} = 7$  and 8 TeV at the LHC ALICE and CMS experiments. It has been concluded [42] that a large enough initial energy density to create a non-hadronic perfect fluid (QGP-like) is available in high-multiplicity proton-proton events at the LHC. The analogous advanced calculations, employing the relativistic hydrodynamic solutions in [43], have yielded  $\epsilon(13 \text{ TeV}) \approx 0.69 \text{ GeV}/\text{fm}^3$  using  $\langle dN_{ch}/d\eta \rangle \approx 6.5$  in minimum bias proton-proton collisions at  $(s)^{1/2} = 13$  TeV at mid- $y$  at the LHC. Assuming the proportionality of the charged-particle multiplicity density to the initial energy density ( $\epsilon$ ) and employing the results of [43], the critical value of  $\langle dN_{ch}/d\eta \rangle$  at mid- $y$  in proton-proton collisions at  $(s)^{1/2} = 13$  TeV, required to achieve the critical QCD energy density ( $1 \text{ GeV}/\text{fm}^3$ ), has been calculated in [21] as follows:

$$\langle \frac{dN_{ch}}{d\eta} \rangle (p + p \text{ at } 13 \text{ TeV}) = \frac{1 \text{ GeV}/\text{fm}^3}{0.69 \text{ GeV}/\text{fm}^3} \cdot 6.5 \approx 9.4 \tag{8}$$

Similarly, using the results of [42], we can evaluate the critical  $\langle dN_{ch}/d\eta \rangle$  at mid- $y$  in proton-proton collisions at  $(s)^{1/2} = 7$  TeV to achieve the critical QCD energy density ( $1 \text{ GeV}/\text{fm}^3$ ):

$$\langle \frac{dN_{ch}}{d\eta} \rangle (p + p \text{ at } 7 \text{ TeV}) = \frac{1 \text{ GeV}/\text{fm}^3}{0.645 \text{ GeV}/\text{fm}^3} \cdot 5.9 \approx 9.1 \tag{9}$$

Our estimate of  $\langle dN_{ch}/d\eta \rangle \approx 6.1 \pm 0.3$  for the probable onset of deconfinement phase transition was found to be lower than the critical value of  $\langle dN_{ch}/d\eta \rangle$  for achieving the QCD critical energy density ( $1 \text{ GeV}/\text{fm}^3$ ), evaluated above (Equation (9)) in collisions of protons at  $(s)^{1/2} = 7$  TeV at mid- $y$ . It is an interesting result that  $\langle dN_{ch}/d\eta \rangle \approx 6.1 \pm 0.3$  for

the probable deconfinement phase transition estimated in the present work in collisions of protons at  $(s)^{1/2} = 7$  TeV proved to be smaller than, but close to, the corresponding  $\langle dN_{ch}/d\eta \rangle \approx 7.1 \pm 0.2$  estimated in [21] in collisions of protons at  $(s)^{1/2} = 13$  TeV, which is also observed in Figure 4a,b. Using the results of Equations (8) and (9), in the present analysis we can estimate the respective critical energy densities for the probable onset of deconfinement phase transition in proton-proton collisions at  $(s)^{1/2} = 7$  and 13 TeV corresponding to  $\langle dN_{ch}/d\eta \rangle \approx 6.1 \pm 0.3$  and  $\langle dN_{ch}/d\eta \rangle \approx 7.1 \pm 0.2$ , respectively:

$$\varepsilon_{tr}(p + p \text{ at } 7 \text{ TeV}) = \frac{6.1}{9.1} \times 1 \frac{\text{GeV}}{\text{fm}^3} \approx 0.67 \pm 0.03 \frac{\text{GeV}}{\text{fm}^3} \quad (10)$$

and

$$\varepsilon_{tr}(p + p \text{ at } 13 \text{ TeV}) = \frac{7.1}{9.4} \times 1 \frac{\text{GeV}}{\text{fm}^3} \approx 0.76 \pm 0.02 \frac{\text{GeV}}{\text{fm}^3} \quad (11)$$

As seen from the above calculations, the estimated critical energy densities for the probable onset of deconfinement phase transitions in proton-proton collisions at  $(s)^{1/2} = 7$  and 13 TeV have proven to be significantly smaller than the critical value of  $1 \text{ GeV}/\text{fm}^3$  from lattice QCD calculations. From the comparison of non-extensivity parameter  $q$  versus  $\langle dN_{ch}/d\eta \rangle$  dependencies for two collision energies in Figure 3a, it has been deduced that the systems produced in collisions of protons at  $(s)^{1/2} = 7$  TeV are characterized by a noticeably larger degree of equilibrium and thermalization as compared to that in proton-proton collisions at  $(s)^{1/2} = 13$  TeV, which could be due to the faster and more violent proton-proton collisions at  $(s)^{1/2} = 13$  TeV than those at  $(s)^{1/2} = 7$  TeV. The deduced larger degree of equilibrium and thermalization at  $(s)^{1/2} = 7$  TeV, compared to that at  $(s)^{1/2} = 13$  TeV, can probably explain our finding that the probable onset of deconfinement phase transition in proton-proton collisions at  $(s)^{1/2} = 7$  TeV takes place at a lower estimated critical energy density ( $0.67 \pm 0.03 \text{ GeV}/\text{fm}^3$ ) than that ( $0.76 \pm 0.02 \text{ GeV}/\text{fm}^3$ ) in collisions of protons at  $(s)^{1/2} = 13$  TeV.

Here, it is worth mentioning the results of relevant works [61–63] of Campanini et al. In an early paper [61], the available experimental data on average  $p_t$  ( $\langle p_t \rangle$ ) versus charged-particle rapidity density,  $dn/dy$ , dependencies in proton-proton and proton-antiproton collisions at SPS collider and ISR have been examined. It has been suggested [61] that evidence may already be available of high-temperature phase transition to quark-gluon plasma in hadronic collision events at SPS and ISR with central rapidity density  $dn/dy$  within one or two units around 6. In [62], it has been shown that in various experiments in proton-proton and proton-antiproton collisions at  $(s)^{1/2}$  energies ranging from 22 GeV to 7 TeV, there is a well-defined slope change in  $\langle p_t \rangle$  versus charged-particle rapidity density, which may indicate a phase transition to a new production mechanism of particles at  $dn/dy = 5.5 \pm 1.2$ . In [63], the approximate equations of state (EOS) have been extracted from the analysis of  $\langle p_t \rangle$  versus  $dN_{ch}/d\eta$  dependencies in experimental data on proton-proton and proton-antiproton interactions at  $(s)^{1/2}$  energies ranging from 31 GeV to 7 TeV. The obtained results [63] proved to be consistent with theory predictions in case of crossover from hadronic gas to quark gluon plasma, starting at  $(dN_{ch}/d\eta) \approx 6$  and ending at  $(dN_{ch}/d\eta) \approx 24$ . Hence, the critical values  $\langle dN_{ch}/d\eta \rangle \approx 6.1 \pm 0.3$  and  $\langle dN_{ch}/d\eta \rangle \approx 7.1 \pm 0.2$  [21] for the probable onset of deconfinement phase transition in collisions of protons at  $(s)^{1/2} = 7$  and 13 TeV, respectively, estimated from the analysis of the dependency of  $T_0$  and  $\langle \beta_t \rangle$  on  $\langle dN_{ch}/d\eta \rangle$ , are consistent and in good agreement with the respective estimates of Campanini, deduced from detailed analyses of the average  $p_t$  ( $\langle p_t \rangle$ ) versus charged-particle (pseudo)rapidity density dependencies in [61–63].

For more precise estimations of the critical  $\langle dN_{ch}/d\eta \rangle$  and corresponding critical energy density for the probable onset of deconfinement phase transition in collisions of protons at high LHC energies, it is necessary to conduct a further comprehensive analysis of dependencies of particle production on  $\langle dN_{ch}/d\eta \rangle$  in proton-proton collisions, preferably with smaller binning in  $\langle dN_{ch}/d\eta \rangle$ .

## 5. Summary and Conclusions

We have analyzed experimental  $p_t$  distributions of particles at ten groups of  $\langle dN_{ch}/d\eta \rangle$  in inelastic proton-proton collisions at  $(s)^{1/2} = 7$  TeV at mid- $y$  at the LHC, measured by ALICE collaboration. We have studied the change of collective characteristics of the collision system with varying  $\langle dN_{ch}/d\eta \rangle$  through combined minimum  $\chi^2$  model fits of  $p_t$  distributions of identified charged particles, using the Tsallis distribution function with thermodynamical consistence and the Hagedorn function with included transverse (radial) flow. The combined minimum  $\chi^2$  fits with the Tsallis function with thermodynamical consistence and the Hagedorn function with transverse (radial) flow quite well-describe the  $p_t$  distributions of the studied particle species in ten different groups of  $\langle dN_{ch}/d\eta \rangle$  in collisions of protons at  $(s)^{1/2} = 7$  TeV. The findings of the present analysis for proton-proton collisions at  $(s)^{1/2} = 7$  TeV were systematically compared with the respective results of recent work [21] for proton-proton collisions at  $(s)^{1/2} = 13$  TeV.

The values of non-extensivity parameter  $q$  for pions and kaons, protons and antiprotons in proton-proton collisions at  $(s)^{1/2} = 7$  TeV were found to be noticeably smaller compared to those in collisions of protons at  $(s)^{1/2} = 13$  TeV in the whole analyzed  $\langle dN_{ch}/d\eta \rangle$  range. This indicates that the systems produced in proton-proton collisions at  $(s)^{1/2} = 7$  TeV have a noticeably larger degree of equilibrium and thermalization than those at  $(s)^{1/2} = 13$  TeV.

The extracted effective temperatures,  $T$ , of the Tsallis function with thermodynamical consistence have shown a consistent increase with the increasing  $\langle dN_{ch}/d\eta \rangle$  in proton-proton collisions at  $(s)^{1/2} = 7$  TeV, in agreement with the similar result [21] obtained in proton-proton collisions at  $(s)^{1/2} = 13$  TeV. The respective  $T$  versus  $\langle dN_{ch}/d\eta \rangle$  dependence in proton-proton collisions at  $(s)^{1/2} = 7$  TeV has been well-described with the simple power function  $T = A \cdot \langle \frac{dN_{ch}}{d\eta} \rangle^a$  with the same value  $\approx 1/3$  of exponent parameter as that obtained recently [21] in proton-proton collisions at  $(s)^{1/2} = 13$  TeV. Comparing the relation  $T \sim \varepsilon^{1/3}$  extracted in the present analysis and in [21] with the relation  $T \sim \varepsilon_\pi^{1/4}$  for the simple model of an ideal gas of massless pions, it was found that dependencies on the initial energy density of the effective temperatures of the systems, created in collisions of protons at  $(s)^{1/2} = 7$  and 13 TeV, and that of an ideal pion gas, are compatible to each other due to the closeness of the corresponding exponent parameters.

It was obtained that the transverse (radial) flow emerged at  $\langle dN_{ch}/d\eta \rangle \approx 6$  and then increased, becoming significant at higher multiplicity events and reaching the maximal value of  $\langle \beta_t \rangle = 0.29 \pm 0.02$  at the highest studied value of  $\langle dN_{ch}/d\eta \rangle = 21.3 \pm 0.6$  in proton-proton collisions at  $(s)^{1/2} = 7$  TeV. These results are consistent with the similar emergence and development of transverse radial flow in larger multiplicity proton-proton events at  $(s)^{1/2} = 13$  TeV at the LHC demonstrated in [21].

We have estimated, analyzing  $T_0$  and  $\langle \beta_t \rangle$  versus  $\langle dN_{ch}/d\eta \rangle$  dependencies, extracted employing the Hagedorn function with included transverse flow, that the probable onset of deconfinement phase transition in proton-proton collisions at  $(s)^{1/2} = 7$  TeV takes place at  $\langle dN_{ch}/d\eta \rangle \approx 6.1 \pm 0.3$ , which is close to the corresponding estimate ( $\langle dN_{ch}/d\eta \rangle \approx 7.1 \pm 0.2$ ) obtained recently in collisions of protons at  $(s)^{1/2} = 13$  TeV in [21]. The critical values  $\langle dN_{ch}/d\eta \rangle \approx 6.1 \pm 0.3$  and  $\langle dN_{ch}/d\eta \rangle \approx 7.1 \pm 0.2$  [21] for the probable onset of deconfinement phase transition in collisions of protons at  $(s)^{1/2} = 7$  and 13 TeV, respectively, estimated by us from the analysis of  $T_0$  and  $\langle \beta_t \rangle$  versus  $\langle dN_{ch}/d\eta \rangle$  dependencies, proved to be consistent and in good agreement with the respective estimates of Campanini et al. in [61–63] and theory predictions [63] in case of crossover from hadronic gas to quark gluon plasma starting at  $(dN_{ch}/d\eta) \approx 6$ . We have also estimated the corresponding critical energy densities for the probable onset of deconfinement phase transitions in proton-proton collisions at  $(s)^{1/2} = 7$  and 13 TeV at the LHC to be  $0.67 \pm 0.03$  and  $0.76 \pm 0.02$  GeV/fm<sup>3</sup>, respectively, being significantly lower than the critical QCD energy density (1 GeV/fm<sup>3</sup>). The noticeably larger degree of equilibrium and thermalization deduced at  $(s)^{1/2} = 7$  TeV than that at  $(s)^{1/2} = 13$  TeV could probably explain our finding that the possible onset of deconfinement phase transition in proton-proton collisions at

$(s)^{1/2} = 7$  TeV takes place at the lower estimated critical energy density ( $0.67 \pm 0.03$  GeV/fm<sup>3</sup>), as compared to that ( $0.76 \pm 0.02$  GeV/fm<sup>3</sup>) in proton-proton collisions at  $(s)^{1/2} = 13$  TeV.

**Author Contributions:** K.K.O., F.-H.L., K.A.M. and M.Z.S. have contributed equally to this work. All authors have read and agreed to the published version of the manuscript.

**Funding:** The work of F.-H.L. has been supported by the National Natural Science Foundation of China under Grant Nos. 11575103, 12047571, and 11947418, and the Shanxi Provincial Natural Science Foundation under Grant No. 201901D111043. The work of Kh.K.O., K.A.M., and M.Z.S. has been supported by the Ministry of Innovative Development of Uzbekistan within the framework of fundamental project No. F3-20200929146 on analysis of open data on proton-proton and heavy-ion collisions at the LHC.

**Data Availability Statement:** The data analyzed in this work are included within the manuscript and cited as references at relevant places within the text of the article.

**Conflicts of Interest:** The authors declare no conflict of interest regarding the article. The funding agencies did not have any role in the design of the study; in collection and analysis of the data; in the interpretation of the results; in the writing of the article, or in the decision to publish the manuscript.

## References

1. Tsallis, C. Possible generalization of Boltzmann-Gibbs statistics. *J. Stat. Phys.* **1988**, *52*, 479. [\[CrossRef\]](#)
2. Tsallis, C. Nonadditive entropy: The concept and its use. *Eur. Phys. J. A* **2009**, *40*, 257. [\[CrossRef\]](#)
3. Cleymans, J.; Worku, D. The Tsallis distribution in proton-proton collisions at  $(s_{nn})^{1/2} = 0.9$  TeV at the LHC. *J. Phys. G* **2012**, *39*, 025006. [\[CrossRef\]](#)
4. Sena, I.; Deppman, A. Systematic analysis of  $p_T$ -distributions in  $p + p$  collisions. *Eur. Phys. J. A* **2013**, *49*, 17. [\[CrossRef\]](#)
5. PHENIX Collab. Measurement of neutral mesons in  $p+p$  collisions at  $(s_{nn})^{1/2} = 200$  GeV and scaling properties of hadron production. *Phys. Rev. D* **2011**, *83*, 052004. [\[CrossRef\]](#)
6. Khandai, P.K.; Sett, P.; Shukla, P.; Singh, V. Hadron spectra in  $p+p$  collisions at RHIC and LHC energies. *Int. J. Mod. Phys. A* **2013**, *28*, 1350066. [\[CrossRef\]](#)
7. Wong, C.Y.; Wilk, G. Tsallis Fits to  $p_T$  Spectra for pp Collisions at LHC. *Acta Phys. Polon. B* **2012**, *43*, 2047. [\[CrossRef\]](#)
8. Cleymans, J.; Lykasov, G.; Parvan, A.; Sorin, A.; Teryaev, O.; Worku, D.S. Systematic properties of the Tsallis distribution: Energy dependence of parameters in high energy  $p-p$  collisions. *Phys. Lett. B* **2013**, *723*, 351. [\[CrossRef\]](#)
9. Cleymans, J. On the Use of the Tsallis Distribution at LHC Energies. *J. Phys. Conf. Ser.* **2017**, *779*, 012079. [\[CrossRef\]](#)
10. Zheng, H.; Zhu, L. Comparing the Tsallis Distribution with and without Thermodynamical Description in  $p-p$  Collisions. *Adv. High Energy Phys.* **2016**, *2016*, 9632126. [\[CrossRef\]](#)
11. Khandai, P.K.; Sett, P.; Shukla, P.; Singh, V. System size dependence of hadron  $p_T$  spectra in  $p+p$  and Au+Au collisions at  $(s_{nn})^{1/2} = 200$  GeV. *J. Phys. G* **2014**, *41*, 025105. [\[CrossRef\]](#)
12. Tsallis, C.; Mendes, R.; Plastino, A.R. The role of constraints within generalized nonextensive statistics. *Phys. A* **1998**, *261*, 534–554. [\[CrossRef\]](#)
13. Biró, T.S.; Purcsel, G.; Ürmössy, K. Non-extensive approach to quark matter. *Eur. Phys. J. A* **2009**, *40*, 325. [\[CrossRef\]](#)
14. Li, L.-L.; Liu, F.-H.; Olimov, K.K. Excitation Functions of Tsallis-Like Parameters in High-Energy Nucleus–Nucleus Collisions. *Entropy* **2021**, *23*, 478. [\[CrossRef\]](#) [\[PubMed\]](#)
15. Olimov, K.K.; Iqbal, A. Systematic analysis of midrapidity transverse momentum spectra of identified charged particles in  $p+p$  collisions at  $(s_{nn})^{1/2} = 2.76, 5.02$ , and 7 TeV at the LHC. *Int. J. Mod. Phys. A* **2020**, *35*, 2050167. [\[CrossRef\]](#)
16. Olimov, K.K.; Kanokova, S.Z.; Olimov, A.K.; Umarov, K.I.; Tukhtaev, B.J.; Gulamov, K.G.; Yuldashev, B.S.; Lutpullaev, S.L.; Saidkhanov, N.S.; Kosim Olimov, K.; et al. Combined analysis of midrapidity transverse momentum spectra of the charged pions and kaons, protons and antiprotons in  $p+p$  and Pb+Pb collisions at  $(s_{nn})^{1/2} = 2.76$  and 5.02 TeV at the LHC. *Mod. Phys. Lett. A* **2020**, *35*, 2050237. [\[CrossRef\]](#)
17. STAR Collab. Strange particle production in  $p+p$  collisions at  $(s)^{1/2} = 200$  GeV. *Phys. Rev. C* **2007**, *75*, 064901. [\[CrossRef\]](#)
18. PHENIX Collab. Identified charged hadron production in  $p+p$  collisions at  $(s)^{1/2} = 200$  and 62.4 GeV. *Phys. Rev. C* **2011**, *83*, 064903. [\[CrossRef\]](#)
19. ALICE Collab. Production of pions, kaons and protons in pp collisions at  $(s)^{1/2} = 900$  GeV with ALICE at the LHC. *Eur. Phys. J. C* **2011**, *71*, 1655. [\[CrossRef\]](#)
20. CMS Collab. Study of the inclusive production of charged pions, kaons, and protons in pp collisions at  $(s)^{1/2} = 0.9, 2.76$ , and 7 TeV. *Eur. Phys. J. C* **2012**, *72*, 2164. [\[CrossRef\]](#)
21. Olimov, K.K.; Liu, F.-H.; Musaev, K.A.; Olimov, K.; Tukhtaev, B.J.; Yuldashev, B.S.; Saidkhanov, N.S.; Umarov, K.I.; Gulamov, K.G. Multiplicity dependencies of midrapidity transverse momentum spectra of identified charged particles in  $p+p$  collisions at  $(s)^{1/2} = 13$  TeV at LHC. *Int. J. Mod. Phys. A* **2021**, *36*, 2150149. [\[CrossRef\]](#)

22. Bíró, G.; Barnaföldi, G.G.; Bíró, T.S.; Ürmösy, K.; Takács, Á. Systematic Analysis of the Non-Extensive Statistical Approach in High Energy Particle Collisions—Experiment vs. Theory. *Entropy* **2017**, *19*, 88. [[CrossRef](#)]
23. Shen, K.; Barnaföldi, G.G.; Bíró, T.S. Hadron Spectra Parameters within the Non-Extensive Approach. *Universe* **2019**, *5*, 122. [[CrossRef](#)]
24. Grigoryan, S. Using the Tsallis distribution for hadron spectra in pp collisions: Pions and quarkonia at  $(s_{nn})^{1/2} = 5\text{--}13000$  GeV. *Phys. Rev. D* **2017**, *95*, 056021. [[CrossRef](#)]
25. Bíró, G.; Barnaföldi, G.G.; Bíró, T.S.; Shen, K. Mass hierarchy and energy scaling of the Tsallis–Pareto parameters in hadron productions at RHIC and LHC energies. *EPJ Web Conf.* **2018**, *171*, 14008. [[CrossRef](#)]
26. Schnedermann, E.; Solfrank, J. Thermal phenomenology of hadrons from 200A GeV S+S collisions. *Phys. Rev. C* **1993**, *48*, 2462. [[CrossRef](#)]
27. STAR Collab. Systematic measurements of identified particle spectra in pp, d+Au, and Au+Au collisions at the STAR detector. *Phys. Rev. C* **2009**, *79*, 034909. [[CrossRef](#)]
28. STAR Collab. Identified particle production, azimuthal anisotropy, and interferometry measurements in Au+Au collisions at  $(s_{nn})^{1/2} = 9.2$  GeV. *Phys. Rev. C* **2010**, *81*, 024911. [[CrossRef](#)]
29. Tang, Z.; Xu, Y.; Ruan, L.; van Buren, G.; Wang, F.; Xu, Z. Spectra and radial flow in relativistic heavy ion collisions with Tsallis statistics in a blast-wave description. *Phys. Rev. C* **2009**, *79*, 051901. [[CrossRef](#)]
30. Lao, H.-L.; Liu, F.-H.; Lacey, R.A. Extracting kinetic freeze-out temperature and radial flow velocity from an improved Tsallis distribution. *Eur. Phys. J. A* **2017**, *53*, 44. [[CrossRef](#)]
31. Bhattacharyya, T.; Cleymans, J.; Khuntia, A.; Pareek, P.; Sahoo, R. Radial flow in non-extensive thermodynamics and study of particle spectra at LHC in the limit of small  $(q-1)$ . *Eur. Phys. J. A* **2016**, *52*, 30. [[CrossRef](#)]
32. Thakur, D.; Tripathy, S.; Garg, P.; Sahoo, R.; Cleymans, J. Indication of a Differential Freeze-Out in proton-proton and Heavy-Ion Collisions at RHIC and LHC Energies. *Adv. High Energy Phys.* **2016**, *2016*, 4149352. [[CrossRef](#)]
33. Olimov, K.K.; Kanokova, S.Z.; Olimov, K.; Gulamov, K.G.; Yuldashev, B.S.; Lutpullaev, S.L.; Umarov, F.Y. Average transverse expansion velocities and global freeze-out temperatures in central Cu+Cu, Au+Au, and Pb+Pb collisions at high energies at RHIC and LHC. *Mod. Phys. Lett. A* **2020**, *35*, 2050115. [[CrossRef](#)]
34. ALICE Collab. Centrality dependence of  $\pi$ , K, and p production in Pb-Pb collisions at  $(s_{nn})^{1/2} = 2.76$  TeV. *Phys. Rev. C* **2013**, *88*, 044910. [[CrossRef](#)]
35. Jiang, K.; Zhu, Y.; Liu, W.; Chen, H.; Li, C.; Ruan, L.; Tang, Z.; Xu, Z. Onset of radial flow in p+p collisions. *Phys. Rev. C* **2015**, *91*, 024910. [[CrossRef](#)]
36. Bashir, I.U.; Bhat, R.A.; Uddin, S. Evidence of collective flow in p-p collisions at LHC. *arXiv* **2015**, arXiv:1502.04185v2.
37. Bashir, I.U.; Parra, R.A.; Bhat, R.A.; Uddin, S. Particle Transverse Momentum Distributions in p-p Collisions at  $(s)^{1/2} = 0.9$  TeV. *Adv. High Energy Phys.* **2019**, *2019*, 8219567. [[CrossRef](#)]
38. ALICE Collab. Enhanced production of multi-strange hadrons in high-multiplicity proton-proton collisions. *Nat. Phys.* **2017**, *13*, 535. [[CrossRef](#)]
39. Tripathy, S. et al.; [ALICE Collaboration]. Energy dependence of  $\phi(1020)$  production at mid-rapidity in pp collisions with ALICE at the LHC. *Nucl. Phys. A* **2019**, *982*, 180. [[CrossRef](#)]
40. Dash, A.K. Multiplicity dependence of strangeness and hadronic resonance production in pp and p-Pb collisions with ALICE at the LHC. *Nucl. Phys. A* **2019**, *982*, 467–470. [[CrossRef](#)]
41. Khuntia, A.; Sharma, H.; Kumar Tiwari, S.; Sahoo, R.; Cleymans, J. Radial flow and differential freeze-out in proton-proton collisions at  $(s)^{1/2} = 7$  TeV at the LHC. *Eur. Phys. J. A* **2019**, *55*, 3. [[CrossRef](#)]
42. Csanad, M.; Csörgő, T.; Jiang, Z.-F.; Yang, C.-B. Initial energy density of  $(s_{nn})^{1/2} = 7$  and 8 TeV p-p collisions at LHC. *Universe* **2017**, *3*, 9. [[CrossRef](#)]
43. Jiang, Z.; Csanád, M.; Kasza, G.; Yang, C.; Csörgő, T. Pseudorapidity and Initial-energy Densities in p+p and Heavy-ion Collisions at RHIC and LHC. *Acta Phys. Pol. B Proc. Suppl.* **2019**, *12*, 261. [[CrossRef](#)]
44. Tripathy, S.; Bisht, A.; Sahoo, R.; Khuntia, A.; Panikkassery Salvan, M. Event shape and multiplicity dependence of freeze-out scenario and system thermodynamics in pro-ton+proton collisions at  $(s_{nn})^{1/2} = 13$  TeV using PYTHIA8. *Adv. High Energy Phys.* **2021**, *2021*, 8822524. [[CrossRef](#)]
45. ALICE Collab. Multiplicity dependence of light flavor hadron production in pp collisions at  $(s_{nn})^{1/2} = 7$  TeV. *Phys. Rev. C* **2019**, *99*, 024906. [[CrossRef](#)]
46. Baker, O.K.; Kharzeev, D.E. Thermal radiation and entanglement in proton-proton collisions at energies available at the CERN Large Hadron Collider. *Phys. Rev. D* **2018**, *98*, 054007. [[CrossRef](#)]
47. Kharzeev, D.E.; Levin, E.M. Deep inelastic scattering as a probe of entanglement. *Phys. Rev. D* **2017**, *95*, 114008. [[CrossRef](#)]
48. Berges, J.; Floerchinger, S.; Venugopalan, R. Dynamics of entanglement in expanding quantum fields. *J. High Energy Phys.* **2018**, *2018*, 145. [[CrossRef](#)]
49. Berges, J.; Floerchinger, S.; Venugopalan, R. Thermal excitation spectrum from entanglement in an expanding quantum string. *Phys. Lett. B* **2018**, *778*, 442. [[CrossRef](#)]
50. Feal, X.; Pajares, C.; Vazquez, R.A. Thermal behavior and entanglement in Pb-Pb and p-p collisions. *Phys. Rev. C* **2019**, *99*, 015205. [[CrossRef](#)]

51. ALICE Collab. Multiplicity dependence of  $\pi$ , K, and p production in pp collisions at  $(s_{NN})^{1/2} = 13$  TeV. *Eur. Phys. J. C* **2020**, *80*, 693. [[CrossRef](#)]
52. Hagedorn, R. Multiplicities, pT Distributions and the Expected Hadron→Quark-Gluon Phase Transition. *Riv. Nuovo Cim.* **1983**, *6*, 1. [[CrossRef](#)]
53. Wilk, G.; Wlodarczyk, Z. Power laws in elementary and heavy-ion collisions. A story of fluctuations and nonextensivity? *Eur. Phys. J. A* **2009**, *40*, 299. [[CrossRef](#)]
54. Wilk, G.; Wlodarczyk, Z. Interpretation of the Nonextensivity Parameter q in Some Applications of Tsallis Statistics and Lévy Distributions. *Phys. Rev. Lett.* **2000**, *84*, 2770. [[CrossRef](#)] [[PubMed](#)]
55. Blankenbecler, R.; Brodsky, S.J.; Gunion, J. Analysis of particle production at large transverse momentum. *Phys. Rev. D* **1975**, *12*, 3469. [[CrossRef](#)]
56. Brodsky, S.; Pirner, H.; Raufeisen, J. Scaling properties of high p<sub>T</sub> inclusive hadron production. *Phys. Lett. B* **2006**, *637*, 58. [[CrossRef](#)]
57. ALICE Collab. Production of charged pions, kaons and (anti-)protons in Pb-Pb and inelastic pp collisions at  $(s)^{1/2} = 5.02$  TeV. *Phys. Rev. C* **2020**, *101*, 044907. [[CrossRef](#)]
58. Mishra, A.N.; Paić, G.; Pajares, C.; Scharenberg, R.P.; Srivastava, B.K. Deconfinement and degrees of freedom in pp and A-A collisions at LHC energies. *Eur. Phys. J. A* **2021**, *57*, 245. [[CrossRef](#)]
59. Becattini, F. An introduction to the statistical hadronization model. In Proceedings of the Quark-Gluon Plasma and Heavy Ion Collisions: Past, Present, Future, Torino, Italy, 8–14 December 2008.
60. Sarkar, S.; Satz, H.; Sinha, B. (Eds.) *The Physics of the Quark-Gluon Plasma: Introductory Lectures*; Springer: Berlin/Heidelberg, Germany, 2010. [[CrossRef](#)]
61. Campanini, R. Quark gluon plasma and multiplicity dependence of transverse momentum in hadronic collisions. *Lett. Al Nuovo Cimento* **1985**, *44*, 343. [[CrossRef](#)]
62. Campanini, R. Possible Signals of new phenomena in hadronic interactions at  $dn/d\eta = 5.5 \pm 1.2$ . *arXiv* **2010**, arXiv:1012.5219.
63. Campanini, R.; Ferri, G. Experimental equation of state in proton-proton and proton-antiproton collisions and phase transition to quark gluon plasma. *Phys. Lett. B* **2011**, *703*, 237. [[CrossRef](#)]